



## The Effects of Longitudinal Dimension in Three-Dimensional Slope Stability Analysis

Kumar, S.<sup>1\*</sup>, Shankar Choudhary, S.<sup>2</sup> and Burman, A.<sup>3</sup>

<sup>1</sup> Ph.D. Instructor, Research Scholar, National Institute of Technology, Patna, India.

<sup>2</sup> Assistant Professor, Department of Civil Engineering, National Institute of Technology, Patna, India.

<sup>3</sup> Associate Professor, Department of Civil Engineering, National Institute of Technology, Patna, India.

© University of Tehran 2023

Received: 10 Jul. 2023;

Revised: 02 Oct. 2023;

Accepted: 13 Nov. 2023

**ABSTRACT:** Of late, three-dimensional slope stability analysis has gained popularity among the geotechnical engineers so that the actual response of slope failure, which essentially occurs in 3D, can be captured. However, three-dimensional slope failure analysis necessitates the proper consideration of the third/longitudinal dimension of the slope. Three-dimensional slope stability analysis can yield erroneous results if inadequate length of the third dimension of the slope is used during analysis. This study employs Bishop's simplified approach to find the minimum length of a 3D soil slope's third/longitudinal direction to be considered during analysis. A parametric study compares the findings of 3D and 2D analyses for different geometries, pore pressure ratios and seismic loading for a cohesive-frictional slope. A total of 15 loading cases have been analyzed to study the convergence behavior of the 3D and 2D Factor of Safety (FS) values for slopes with different inclination angles and longitudinal length-to-height (l/h) ratios. The results presented in this study dictate that the longitudinal/third dimension of a 3D slope model should be at least five times the slope's height for accurate 3D slope analysis. For all loading situations, whether a slope will collapse at the base or toe and the failure mass volumes are estimated. As the base inclination angle increases for a particular slope, the type of failure gradually shifts from base failure to toe failure. The volume of failure mass is seen to follow a decreasing trend with an increase in the slope angle.

**Keywords:** Limit Equilibrium Method, Safety Factor, Slope Angle, Bishop's Simplified Method, Critical Failure Surface.

### 1. Introduction

Problems with the stability of slopes are widespread in many civil engineering projects. Construction of large and important projects like embankments, dams, and highways often requires slope

stability analysis (Komasi and Beiranvand, 2021; Kalantari and Pourkhosravani, 2011; Soralump et al., 2021). The failure of a slope can cause enormous economic and social losses. The Limit Equilibrium (LE), Strength Reduction Technique based on Finite Element (FE), and Limit Analysis

\* Corresponding author E-mail: [sumitk.phd19.ce@nitp.ac.in](mailto:sumitk.phd19.ce@nitp.ac.in)

(LA) methods are the most common procedures adopted for analyzing soil slopes (Liu et al., 2020; Qi et al., 2021; Su and Shao, 2021; Wang et al., 2019).

Limit equilibrium procedures have been extensively used in the past as well as in the present day to determine the slope Safety Factor (FS) against failure (Bishop, 1955; Janbu, 1973) and it remains the most preferred method of slope analysis.

Initially, a slope's stability check was formulated in two dimensions (2D), assuming plane strain conditions existed. However, in many situations where the section changes along the longitudinal direction of the slope, the plane strain assumption loses its validity. In such cases, a Three-Dimensional (3D) slope stability analysis is desirable to obtain the correct failure mechanism. In the majority of instances, the width-to-height ratio of the slope is insufficient and varies perpendicular to the movement of the slide.

Therefore, applying 2D studies to 3D problems is not correct but is considered conformist because the end effects are ignored. So, a 2D slope analysis is noticeably conservative when a 3D failure is expected and commonly chosen in the design (Cornforth, 2005). The Limit Equilibrium Method (LEM) remains the most preferred method for analyzing slope stability, despite introducing more advanced numerical methods (Lorig, 1999; Zheng et al., 2018). In reality, though, the failure surfaces of all slope failures are 3D, especially for landslides or natural slopes. Because of this, 3D slope analyses are getting more and more attention with simultaneous advancement in the storage and computing power of modern-day computers. Several researchers presented a detailed and comprehensive account of slope stability analysis (Duncan, 1996; Kumar et al., 2022, 2023). Several processes that account for the third dimension were created by extending their 2D equivalents. Based on the conventional method of slices, many researchers (Baligh and Azzouz, 1975) investigated the slip

surface of a cylinder of limited length with either ellipsoids or cones attached to its ends. Hungr (1987); Chakraborty and Goswami (2021); Johari and Mousavi (2019); Rao et al. (2023); Tozato et al. (2022) had all come up with other 3D methods that are also 3D extensions of limit equilibrium methods.

These methods partly meet equilibrium conditions; in this case, the static indeterminate state would not hold if the failure mass had a symmetrical plane. It is recommended to perform a 3D analysis when performing a back analysis of a slope failure to ensure that the shear strength calculated in the back correctly represents the shear force under three-dimensional loading conditions (Arellano and Stark, 2000). The backwards-calculated shear strength can then be used to fix failed slopes or to design slopes at sites with identical circumstances. The back-calculated shear strengths might be excessively high or unconservative if the 3D end effects are not incorporated. The limit analysis method examines the analysis of slope in terms of energy balance and the analysis findings are quite accurate. The upper bound LA uses a kinetically admissible velocity field to establish the slope failure mechanism (Qin and Chian, 2018; Wang et al., 2020). The upper bound theorem of LA has been employed to assess slope stability because no assumptions regarding interaction forces and predetermined failure surfaces are required (Michalowski, 2002). Limit Finite Element Analysis (LFEA) was also used to study the slope stability problem. Complex slope geometry and constitutive relationships have been taken into account by many researchers (Loukidis et al., 2003).

The lower bound theorem is appealing because it provides a safe estimate of the load capacity of the slope domain by assuming a rigid plastic material model based on an associated flow rule and most published works show that LA method usually involves finite element discretization of slope problem under consideration. This leads to an optimization

problem with large, sparse constraint matrices (Lyamin and Sloan, 2002).

Many researchers performed 3D slope stability analysis based on an upper bound of the LA method (He et al., 2019; Qian et al., 2019; Wang et al., 2020).

Based on the strength reduction approach, the FEM and Finite Difference (FD) methods, which are undoubtedly superior for deformation studies, have also been applied for slope stability evaluation (Dawson and Roth, 2020; Lin et al., 2020; Yuan et al., 2020). During 3D slope stability analysis, one primary concern is to consider the sufficient extent of the longitudinal dimension of the three-dimensional slope model. If the insufficient length of the longitudinal dimension of the 3D slope model is considered, the analyses will fail to reflect the effects of the third dimension correctly. Chakraborty and Go Swami (2021) recommended that the ratio of the third dimension to the slope's height should be greater than four. These analyses were conducted using 3D LEM using SLIDE 3 software for drained and undrained soil.

The lower bound study performed by Li et al. (2010) showed that 2D solutions could be considered in place of 3D solutions for the preliminary design of the slope when  $l/h > 5$ . These findings apply to cohesive-frictional drained slopes and purely cohesive undrained slopes. Additionally, this is comparable to the results of Chugh (2003), who analysed frictional soil slopes.

Michalowski and Martel (2010) demonstrated that the suggested 3D FS becomes constant when  $B/H = 5.0$ , where  $H$ : is the slope's height, and  $B$ : is its longitudinal length. Based on the studies of previous works related to fixing the length of longitudinal dimension during 3D slope, it is evident that researchers did not consider the effects of pore pressure and seismic loadings.

Usually, the nature of critical failure surface changes as these loadings comprises the loading pore pressure ratio and horizontal earthquake loading. In the present work, a parametric analysis is

conducted to determine the significance of 3D longitudinal/end effects by examining the results of 3D and 2D analyses for various geometries, pore pressure ratios and horizontal earthquake loading for cohesive-frictional Slope.

This study aims to establish the minimum extent of the third/longitudinal dimension that must be considered during 3D slope stability analysis for different loading combinations.

## 2. Research Significance

During a 3D slope stability study, an important consideration is the adequate incorporation of the longitudinal dimension in the three-dimensional slope model. If the longitudinal dimension of the 3D slope model is not adequately fixed, the results of 3D slope analyses will be highly erroneous.

The existing literature on this subject reveal that the effects of only gravity loading has been considered while recommending the required extent of the third dimension of the slope during 3D slope analyses. The effects of other loading parameters such as pore pressure and seismic loading were not accounted for while estimating the required length of the third dimension of the slope. To address these issues, researchers employed various geometries, pore pressure ratios, and horizontal earthquake loading for cohesive-frictional slope.

## 3. Slope Stability Analysis

This study aims to determine the minimum extent of the third/longitudinal dimension that should be considered during 3D slope stability analysis. While carrying out 3D slope analysis, if the insufficient length of the longitudinal dimension of the slope is considered, it will lead to an incorrect estimation of 3D FS values. Hence, determining the correct minimum longitudinal dimension during 3D slope analysis is paramount. To assess the minimum length of longitudinal dimension

of the slope needed for 3D slope analysis, the convergence behaviour of the ratio of FS values in two and three dimensions are studied against different values of  $l/h$  where  $l$  and  $h$ : represent the longitudinal dimension of a 3D slope and the height of the slope, respectively (refer to Figure 1a). The 2D geometry of slope is shown in Figure 1b. In this study, different slope stability problems are solved in 2D and 3D based on Bishop's method to derive 2D and 3D FS values against sliding. 2D slope stability analyses were carried out using Slope/W software to find the minimum FS of known shear strength parameters along the failure plane. Slope/W permits various methods to determine the factor of safety, but Bishop's Simplified Method (BSM) is used for the the current work. For 3D slope stability, analyses were carried out using the Scoops 3D source program. The investigations have been performed for different slope angles ( $\beta$ ).

### 3.1. 2D FS Determination Using BSM

In this study, the factor of safety of a 2D slope is determined using Slope/W software which permits various methods to determine factor of safety. But in this research work, a well-known limit equilibrium method, i.e., BSM, is used.

This method ensures moment equilibrium of the failure mass is satisfied with any rotation point. Figure 2 represent the free-body diagram of  $i^{\text{th}}$  slice subjected to all possible combination of forces. In Figure 2,  $W_i$ : is weight of the  $i^{\text{th}}$  slice,  $N_i'$ : is the effective normal force at the base of the  $i^{\text{th}}$  slice,  $S_{mi}$ : is the mobilized shear force at the base of the  $i^{\text{th}}$  slice,  $E_{L_i}$ : is the interslice normal force acting on the  $i^{\text{th}}$  slice from the left direction,  $E_{R_i}$ : is the interslice normal force acting on the  $i^{\text{th}}$  slice from right direction,  $V_{L_i}$ : is interslice shear force acting on the  $i^{\text{th}}$  slice from left direction,  $V_{R_i}$ : is interslice shear force acting on the  $i^{\text{th}}$  slice from right direction,  $k_h$ : is horizontal earthquake coefficient,  $dx$ : is width of each slice,  $\beta_i$ : is the length of base of the  $i^{\text{th}}$  slice,  $Z_{L_i}$ : is the perpendicular distance of  $E_{L_i}$  from center of rotation,  $Z_{R_i}$ : is perpendicular distance of  $E_{R_i}$  from center of rotation,  $x_i$ : is horizontal distance of the center of  $i^{\text{th}}$  slice from center of rotation,  $e_i$ : is the vertical distance of center of  $i^{\text{th}}$  slice from center of rotation,  $r_i$ : is the perpendicular distance of  $N_i'$  from center of rotation.

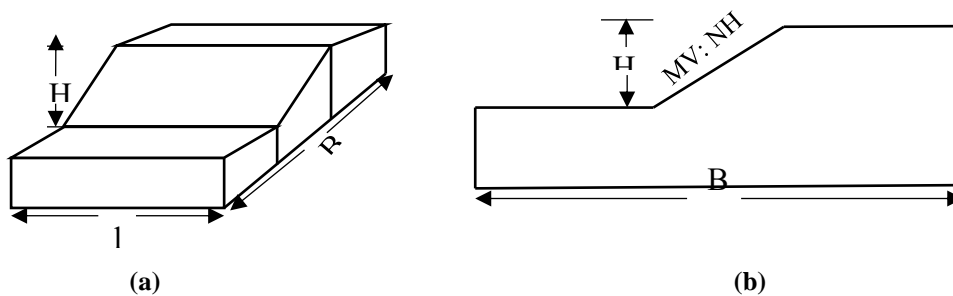


Fig. 1. a) 3D geometry of soil slope; and b) 2D geometry of soil slope

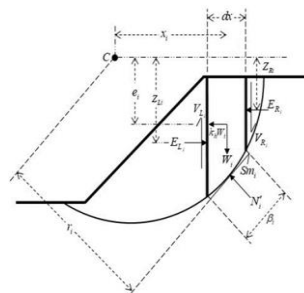


Fig. 2. Free body diagram of  $i^{\text{th}}$  slice

Bishop’s simplified method’s final FS expression considering the effects of pore pressure and earthquake forces, is obtained by satisfying the moment equilibrium condition for sliding mass about its center of rotation, given in Eq. (1).

$$\text{Factor of Safety (FSm)} = \frac{\sum_{i=1}^{n \text{ slices}} \left[ (c'_i \beta_i + (N_i - u_i \beta_i) \tan \phi'_i) r_i \right]}{\sum_{i=1}^{n \text{ slices}} [W_i x_i + k_h W_i e_i - N_i f_i]} \quad (1)$$

If a circular failure surface is considered,  $f_i = 0.0$  in the above expression. Also, the term  $u_i$ : represents the pore water pressure acting on the base of  $i^{\text{th}}$  slice. In order to determine the pore pressure  $u$ , it is necessary to know about the height piezo metric surface of the water. In the absence of such information, an alternative approach to determine pore pressure can be adopted in terms of pore pressure ratio ( $r_u$ ) defined as:

$$r_u = \frac{u}{\gamma z} \quad (2)$$

Therefore, the expression of FS, in terms of  $r_u$ , is expressed as follows:

$$\text{Factor of Safety (FS)} = \frac{\sum_{i=1}^{n \text{ slices}} \left[ \left( c'_i \beta_i + \left( N_i - \frac{W_i r_u}{d_x} \beta_i \right) \tan \phi'_i \right) r_i \right]}{\sum_{i=1}^{n \text{ slices}} [W_i x_i + k_h W_i e_i - N_i f_i]} \quad (3)$$

where  $N_i$ : is the normal force acted at the base of the slice and obtained from the following relation:

$$N_i = \frac{W_i - \left[ c'_i - \frac{W_i r_u \tan \phi'_i}{d_x} \right] \beta_i \sin \alpha_i}{\cos \alpha_i + \frac{\tan \phi'_i \sin \alpha_i}{FS}} \quad (4)$$

where  $\cos \alpha_i + \frac{\tan \phi'_i \sin \alpha_i}{FS} = m_{\alpha i}$  and  $C'$ : is the effective cohesion of soil,  $\phi'_i$ : is the effective shearing resisting of soil. Also, the summation of the difference between the normal forces over the failure mass, i.e.,  $\sum (E_{Ri} - E_{Li})$  as well as the summation of shear forces acting on the sides of the columns, i.e.,  $\sum (V_{Ri} - V_{Li})$  are equated to zero.

### 3.2. 3D formation of BSM

In this work, the FS of a 3D slope is computed using a Scoops 3D-based computer program. While Scoops 3D provides both Ordinary and Bishop simplified methods for calculating the factor of safety, this study uses Bishop’s simplified technique for the assigned problem. Figure 3 illustrates the schematic representation of the free body diagram corresponding to the  $j, k$  column, depicting a scenario in which no external force influences the column while subjected to various force combinations.

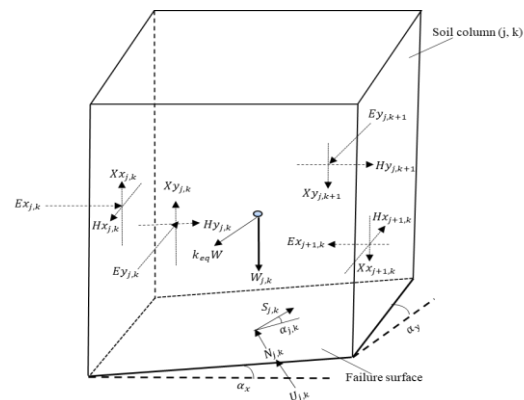


Fig. 3. Illustrating the forces acting on the  $j, k$  column

In Figure 3,  $W$ : is column’s weight,  $E_{x,j,k}, E_{y,j,k}$ : denote  $x$  and  $y$  directions’ inter-column normal force, respectively;  $H_{x,j,k}, H_{y,j,k}$ : signify horizontal shear forces in the  $y$ - $z$  plane,  $X_{x,j,k}, X_{y,j,k}$ : represent the inter-column shear forces in the  $x$  and  $z$  directions, respectively,  $N_{j,k}, U_{j,k}$ : refer to the effective normal force and the pore water force;  $S_{j,k}$ : is the mobilized shear force acting on the

column's base;  $\alpha_{j,k}$ : is the slide angle relative to the x-y plane;  $\alpha_x, \alpha_y$ : are the base inclination in the x-z and y-z planes, respectively, at the midpoint of each column. The Scoops 3D program uses the 3D modification of Bishop's 2D formulation, as suggested by earlier studies. The vertical normal force component is found using the vertical force equilibrium equation for a single column (Hung, 1989) in terms of the trial surface dip angle at the column's base. Moment equilibrium must be maintained according to Bishop's method by equating the global resisting moment to the driving moment. It has been possible to derive the global moment equilibrium for all columns using Eq. (5).

$$\sum M = \sum R_{j,k} \frac{c_{j,k} A_{j,k} + (N_{j,k} - u_{j,k} A_{j,k}) \tan \phi_{j,k}}{FS} - \sum W_{j,k} R_{j,k} m_z \quad (5)$$

The vertical force of the equation, as given in Eq. (6), is used to compute the normal force.

$$N_{j,k} = \frac{W_{j,k} - c'_d A_{j,k} m_z + u_{j,k} A_{j,k} \tan \phi'_d m_z}{\cos \varepsilon_{j,k} + \tan \phi'_d m_z} \quad (6)$$

where,  $\cos \varepsilon_{j,k} + \tan \phi'_d m_z = m_{\alpha_{j,k}}$ ;  $c'_d = \frac{c_{j,k}}{FS}$ ;  $\tan \phi'_d = \frac{\tan \phi_{j,k}}{FS}$  and  $m_z = \sin \alpha_{j,k}$

Bishop's simplified method's final safety factor expression can be computed as a function of  $r_u$  as expressed in Eq. (7).

$$FS = \frac{\sum R_{j,k} (c_{j,k} A_{j,k} + W_{j,k} (1 - r_{u_{j,k}}) \tan \phi_{j,k}) / m_{\alpha_{j,k}}}{\sum W_{j,k} [R_{j,k} m_z + k_{eq} e_{j,k}]} \quad (7)$$

where,  $c_{j,k}$ : is the effective cohesion of soil,  $\phi_{j,k}$ : is the soil friction angle,  $R_{j,k}$ : is the distance between the trial slip region and the rotation axis of the  $j,k$  column;  $N_{j,k}$ : is the column's normal force;  $r_{u_{j,k}}$ : is pore pressure ratio;  $A_{j,k}$ : is the column's trial surface area,  $W_{j,k}$ : is the column's weight,  $\alpha_{j,k}$ : is the apparent dip angle between the azimuthal and slip directions, as shown in Figure 3.

### 3.3. 2D and 3D Slope Geometry Design

For both 2D and 3D slope assessments, the geometry of the domain must be set up first. A method called the Entry and Exit approach is used in 2D slope stability analysis to determine the critical failure surface and associated minimum factor of safety. In Figure 4a, two thick (red) lines run along the ground, representing the range of entry points of the slip circles, whereas the red line on the upper surface represents the range of exit points of the slip circles.

The number of entry and exits can be calculated by specifying increments along these two lines. As seen in Figure 4b, the 2D slip circle comprises vertical slices. In Scoops-3D software, the three-dimensional slope profile is performed using the Digital Elevation Modelling (DEM) technique. DEM is a digital representation of the topographic relief. DEMs are extensively utilized in the field of geomorphology because of their ability to accurately depict diverse landscape features. Regular grids are widely found in the field of digital DEMs and are available in many forms (Xu et al., 2022).

The precision of a DEM is impacted by a range of topographical characteristics, including landforms, altitudes, roughness, and vegetation. The column width, often known as the DEM cell size, is specified by the user. Surface elevation data for DEM cells is included in DEM input files.

The Box Search Method is used in three-dimensional slope stability investigations to find the critical failure surface and calculate the related minimal FS. Figure 5a depicts a three-dimensional search lattice displaying a DEM profile, whereas Figure 5b depicts the DEM cells from a plan perspective. Throughout the search process, Scoops 3D maintains a record of the minimum safety factor computed for each DEM cell among all trial surfaces encompassing that cell.

Each trial surface must be a part of a sphere with a rotational centre point above the DEM and a given radius. So, this helps the search process.

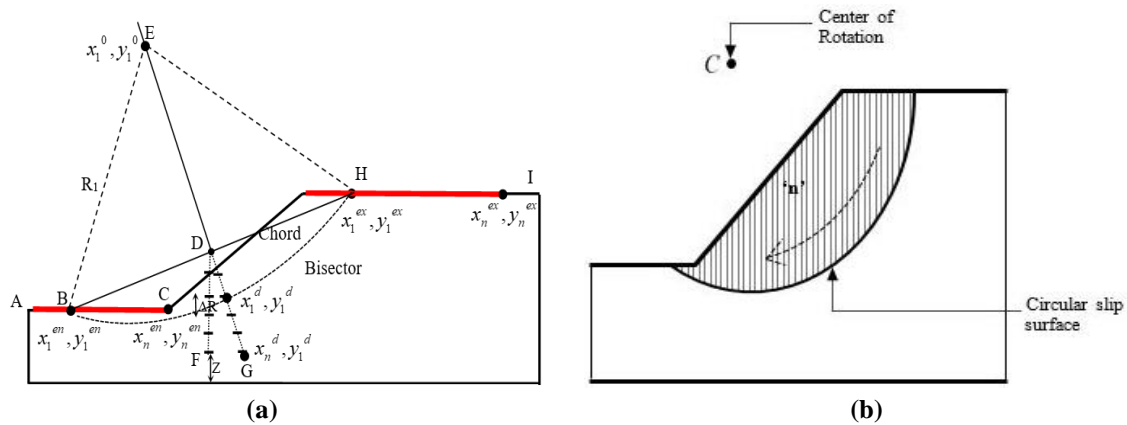


Fig. 4. a) Trial-slip entry and exit areas; and b) 2D slope profile with vertical slice

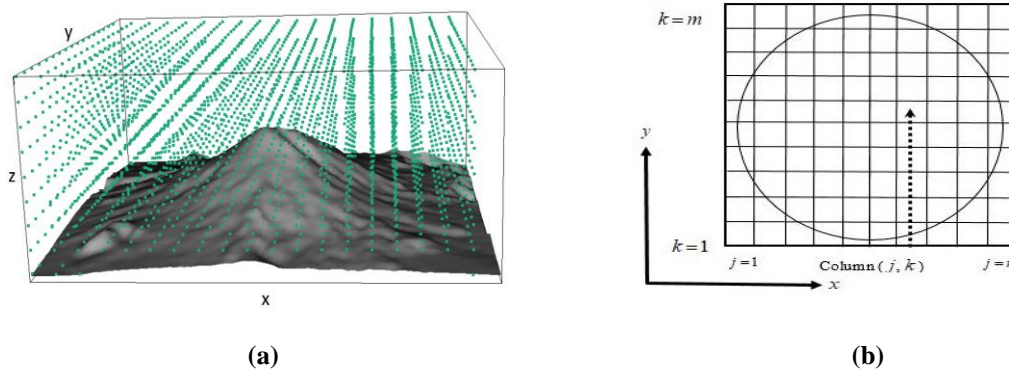


Fig. 5. a) 3D search region of a DEM profile (Reid et al., 2015); and b) Potential sliding mass divided in vertical columns

### 3.4. Role of longitudinal Extent in 3D Slope Analysis

A parametric study is carried out to examine the importance of 3D longitudinal/end effects by comparing the results of 3D and 2D analyses for different geometries, pore pressure ratio, horizontal earthquake loading and same shear strength parameters along the failure surface. A problem from Arai and Tagyo (1985) work is selected to illustrate the use of parametric research results and the significance of doing a 3D analysis in practice. In this study, the aim is to investigate the convergence behavior of the ratio of the 3D/2D factor of safety in the longitudinal direction, which will help to fix the longitudinal dimension's extent of a 3D slope. At different  $l/h$  ratios and for different slope angles, the ratio of 3D and 2D FS values are examined and the  $l/h$  ratio at which  $FS_{3D}/FS_{2D}$  attains constant value is chosen to fix the minimum extent of the longitudinal dimension of the 3D slope. The

ratio of 3D and 2D factor of safeties is expressed as follows:

$$\eta = \frac{FS_{3D}}{FS_{2D}} \tag{8}$$

### 3.5. Validation of the 2D and 3D Slope Stability Analysis Results

Table 1 demonstrates that the results of the 2D and 3D slope analysis of homogeneous soil with no water table and earthquake loading, developed with Slope/W software and Scoops 3D computer code, match the published results. This exercise determines the validity and precision of the Slope/W and Scoops 3D computer programs. When performing 3D slope analysis, the longitudinal extent of the 3D domain must be fixed correctly in 3D. It is typically accomplished through trial and error by ensuring that the 3D FS value does not change after modifying the slope's longitudinal dimension.

**Table 1.** Computed 2D and 3D fs with previously reported results

Reference	H (m)	$\beta$ (°)	$c'$ (kN/m <sup>2</sup> )	$\phi'$ (°)	$\gamma'$ (kN/m <sup>3</sup> )	FS (2D)	FS (3D)	Present study (2D)	Present study (3D)
Arai and Tagyo (1985)	20	33.69	41.65	15	18.816	1.401	-	1.405	-
Reid et al. (2015)	10	26.56	3	19.60	20	0.99	1.04	0.986	1.03
Deng et al. (2015)	20	33.7	42.7	0	18.82	-	1.42	-	1.44
Huang et al. (2002)	12.2	26.5	28.7	20	18.84	-	2.22	-	2.23

For a given height of the slope  $H$ , and the length of the slope  $B$  in the longitudinal direction, previous research (Deng et al., 2015; Xie et al., 2006), demonstrates that the predicted 3D FS becomes constant

#### 4. Results and Discussion

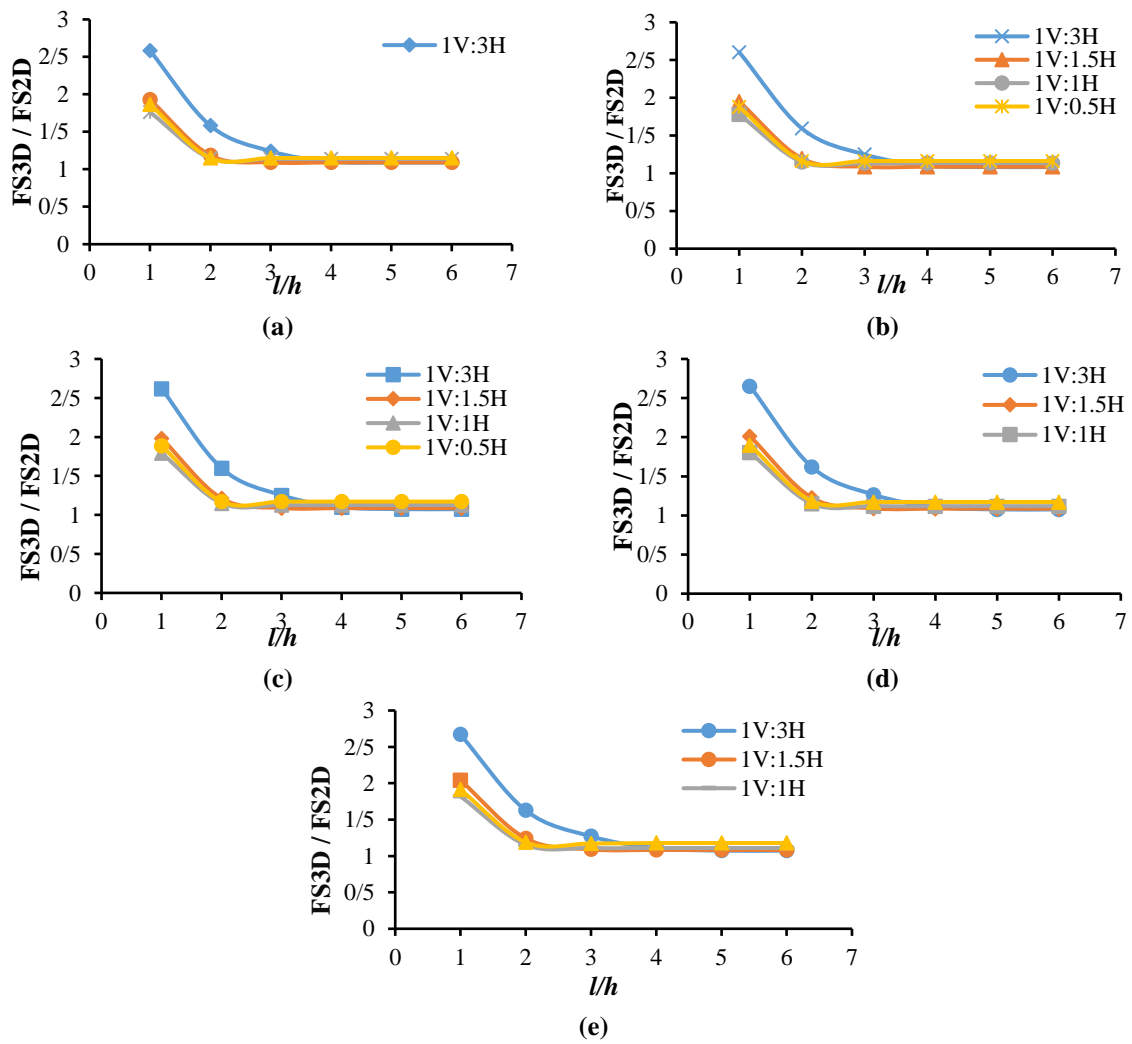
In order to investigate the convergence behavior of the ratio of FS<sub>3D</sub> and FS<sub>2D</sub>, a soil slope with homogenous material properties is chosen. The material properties considered are effective cohesion  $c' = 41.65$  kN/m<sup>2</sup>, effective internal friction angle  $\phi' = 15^\circ$  and unit weight  $\gamma' = 18.816$  kN/m<sup>3</sup> and height of the slope  $h = 20.0$  m. Arai and Tagyo (1985) had already analyzed a 1V:1.5H homogenous slope with the same material properties. However, a total of four geometric configurations of the slope i.e., 1V:3H, 1V:1.5H, 1V:1H and 1V:0.5H, are analyzed to estimate the 3D and 2D FS ratios i.e.,  $\eta$  values as defined in Eq. (6) in the present work. Here,  $V$  and  $H$ : denote the slope's vertical and horizontal dimensions, respectively. All these slope problems are analyzed for different loading combinations involving pore pressure and earthquake loadings. The pore pressure loadings on the slope are simulated considering 3 values of pore pressure ratio i.e.,  $r_u = 0.0, 0.25$  and  $0.50$ . Similarly, the seismic loading on the slope is simulated by applying an equivalent horizontal static loading. For the 2D case, a slice is subjected to horizontal force of value  $k_h w_i$ , where  $k_h$ : is called the pseudo-static horizontal seismic coefficient. In 3D analysis, the same

when  $B/H = 4.0$ . In all instances of 3D slope stability problems, it is a requirement that the width of the third dimension ( $B$ ) be set to a minimum of four times the height ( $H$ ) of the slope.

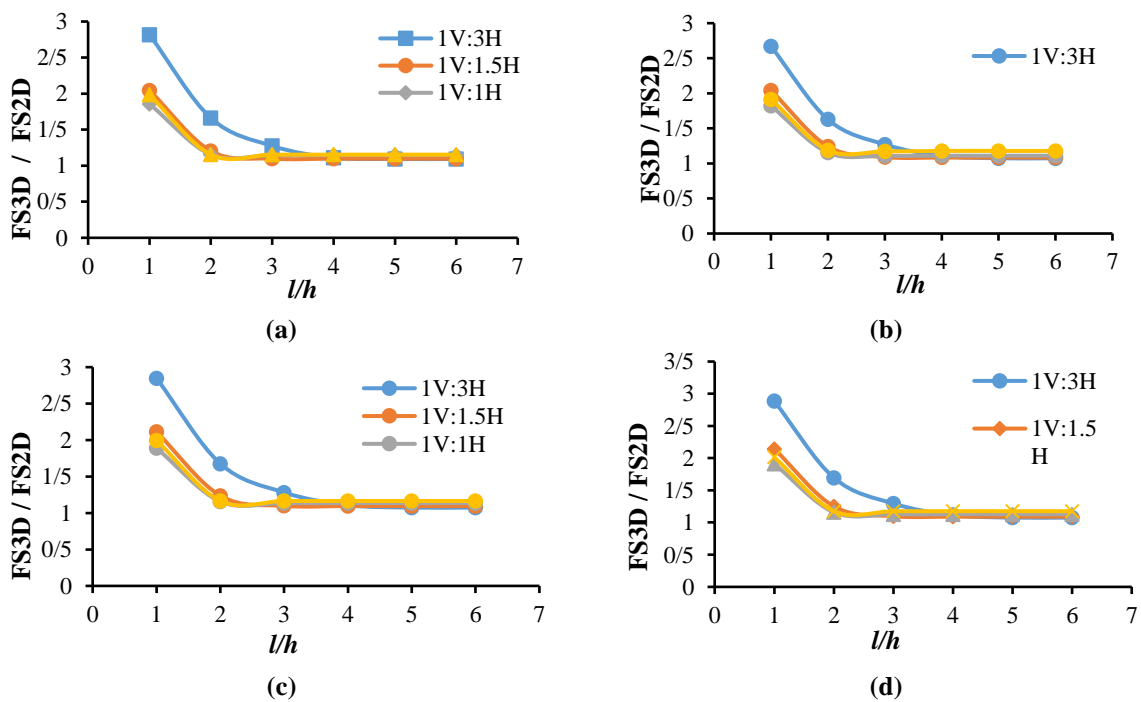
horizontal seismic coefficient is denoted as  $k_{eq}$ , as evident from Eq. (5). The different values of  $k_h$  and  $k_{eq}$  considered in the present analyses are: 0.0, 0.05, 0.10, 0.15 and 0.20, respectively. Overall, 15 loading combinations have been considered in the current work, out of which the case  $r_u = 0.0$  and  $k_h = k_{eq} = 0.0$  represents a soil slope subjected to only gravity loading. Figures 6a-6e present the ratio of the 3D factor of safety to the 2D factor of safety, i.e., the  $\eta$  values considering pore pressure ratio  $r_u = 0.0$  and different pseudo-static horizontal seismic coefficients  $k_h = k_{eq} = 0.0, 0.05, 0.10, 0.15$  and  $0.20$  with varying inclinations of slopes (1V:3H, 1V:1.5H, 1V:1H and 1V:0.5H) as well as for different  $l/h$  ratios (where  $l$ : is the length in the longitudinal direction and  $h$ : is the height of the slope). For 1V:3H slope or slope angle  $\beta = 18.43^\circ$ , it is observed that the parameter  $\eta$  converges at a  $l/h$  value equal to 5.0 or more. When the slope angle  $\beta$  is high, it is noticed that the ratio of the safety factor, i.e.,  $\eta$  converges faster and becomes almost constant at  $l/h = 3.0$  or more.

Similarly, the variation of  $\eta$  values against different  $l/h$  ratios is presented for  $r_u = 0.25$  and  $r_u = 0.50$ , considering the same set of  $k_h = k_{eq} = 0.0, 0.05, 0.10, 0.15$  and  $0.20$  values in Figures 7a-7e and 8a-8e, respectively.





**Fig. 6.** Influence of  $l/h$  on the ratio of 3D/2D FS for condition and: a)  $r_u = 0, k_{eq} = 0.0$ , b)  $r_u = 0, k_{eq} = 0.05$ ; c)  $r_u = 0, k_{eq} = 0.10$ ; d)  $r_u = 0, k_{eq} = 0.15$ ; and e)  $r_u = 0, k_{eq} = 0.20$



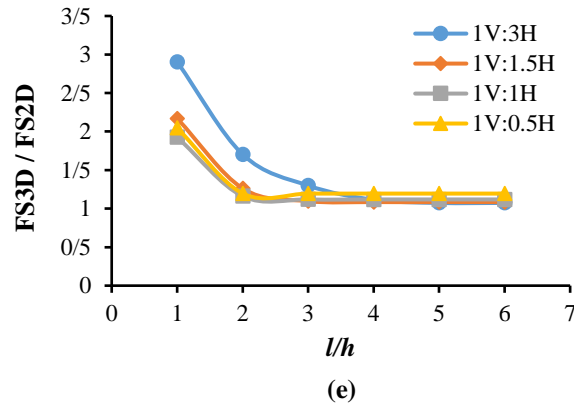


**Fig. 7.** Influence of  $l/h$  on the ratio of 3D/2D FS for condition and: a)  $r_u = 0.25, k_{eq} = 0.0$ ; b)  $r_u = 0.25, k_{eq} = 0.05$ ; c)  $r_u = 0.25, k_{eq} = 0.10$ ; d)  $r_u = 0.25, k_{eq} = 0.15$ ; and e)  $r_u = 0.25, k_{eq} = 0.20$

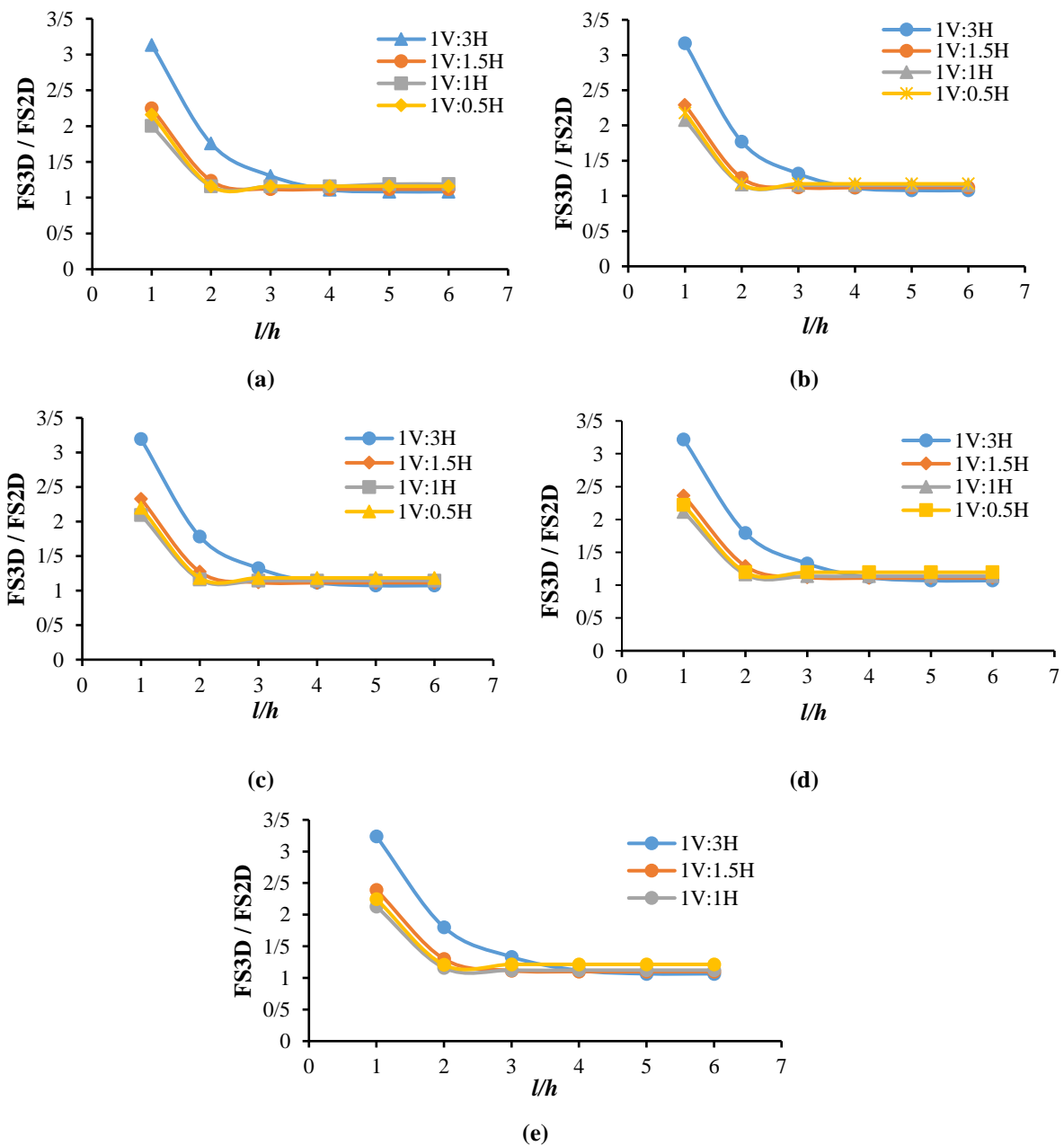


**Fig. 8.** Influence of  $l/h$  on the ratio of 3D/2D FS for condition and: a)  $r_u = 0.50, k_{eq} = 0.0$ ; b)  $r_u = 0.50, k_{eq} = 0.05$ ; c)  $r_u = 0.50, k_{eq} = 0.10$ ; d)  $r_u = 0.50, k_{eq} = 0.15$ ; and e)  $r_u = 0.50, k_{eq} = 0.20$

In this case, similar observations regarding the convergence of FS3D and FS2D ratios can be made i.e.,  $\eta$  values converge when the longitudinal dimension  $l$  is at least equal to  $5h$ . Therefore, in general, it can be stated the longitudinal dimension  $l$  should at least be considered five times the height of the slope ( $h$ ) to obtain correct 3D FS values.

It is further observed that both 3D and 2D safety factor values decrease with an increase in slope angle  $\beta$ . It is also noted that there is a decrease in the safety factor for both 2D and 3D FS values as the pore pressure ratio increases. However, it has also been observed that an increase in pseudo-static horizontal seismic coefficients leads to a decrease in the safety factor for both 2D and 3D analyses. In most loading scenarios, the ratio FS3D/FS2D is seen to converge at  $l/h = 4.0$ . However, for the geometric configuration 1V:3H and loading level  $r_u = 0.50$ ,  $k_{eq} = 0.20$ , it is seen that FS3D/FS2D ratio achieves desired level of convergence at  $l/h > 4.0$ .

Hence, it is preferred a safe choice of the extent of the third/longitudinal dimension of the slope equaling the 5 times the height of the slope. Studying the nature of 3D failure surfaces for all the loading conditions mentioned earlier is necessary. The present paper considers four different geometric configurations of the slope, i.e., 1V:3H, 1V:1.5H, 1V:1H, and 1V:0.5H. The slope angles for these cases are  $\beta = 18.43^\circ$ ,  $33.69^\circ$ ,  $45.0^\circ$  and  $63.43^\circ$ , respectively. The analysis performed using  $l/h = 5.0$  shows these critical failure surfaces. Figures 9-12 present the Critical Failure Surface (CFS) with minimum FS values obtained from 3D slope analysis. From Figures 9 and 10, the nature of slope failure is identified as a base failure for slopes with  $\beta = 18.43^\circ$  and  $33.69^\circ$ . Figures 10 and 11 show that for  $\beta = 45.0^\circ$  and  $63.43^\circ$ , the nature of CFS corresponds to toe failure. Therefore, an observation can be made that the nature of CFS gradually transitions towards toe failure from base failure as the slope angle  $\beta$  increases.

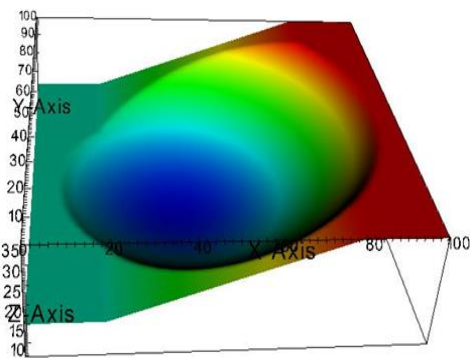


Fig. 9. 3D critical failure surface for slope 1V:3H

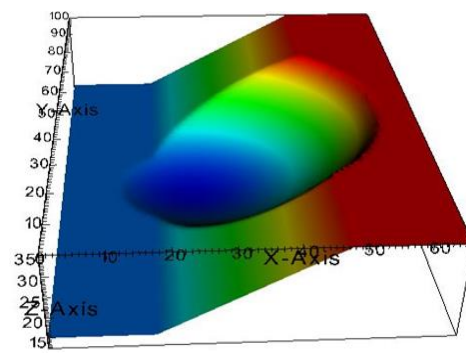


Fig. 10. 3D critical failure surface for slope 1V:1.5H

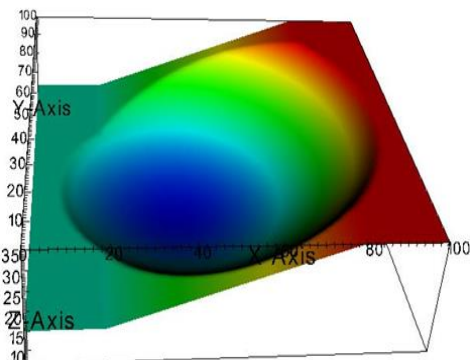


Fig. 11. 3D critical failure surface for slope 1V:1H

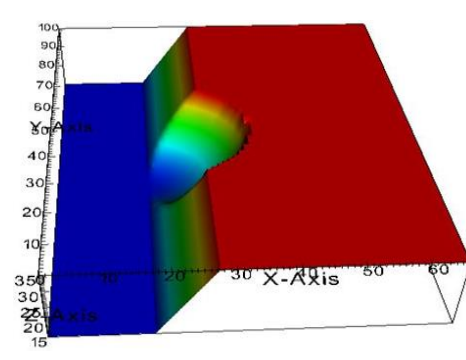


Fig. 12. 3D critical failure surface for slope 1V:0.5H

The corresponding values of the 3D and 2D minimum safety factors are presented in Table 2 for different slope angles, pore pressure ratios, and horizontal earthquake loading combinations. A LEM-based, simplified Bishop's method calculates the minimum safety factors. For various parametric studies, the 2D safety factor is determined using the Slope/W software, while the 3D safety factors are determined using the Scoops 3D computer program. Table 2 only shows the FS3D values for  $l/h = 5.0$ , as the FS3D values computed for these geometric configurations of the 3D slope show desirable convergence. The safety factor values exhibit a negative correlation with the slope angle, as indicated in Table 2.

It is observed that safety factor values decrease with increased pore pressure ratio and horizontal earthquake loading, as presented in Table 2. It is also verified that the 2D safety factor of a simple slope (1V:1.5H) chosen by Arai and Tagyo (1985) is well matched in this study using Slope/W software. It can be further observed that the failure mass/volume decrease as the slope angle  $\beta$  increases. This fact corresponds to the lowering of the resisting forces, as the resisting forces are usually calculated for the entire failure mass. As a result, it can be stated that when the slope angle  $\beta$  increases, there is an overall decrease in the factor of safety value against sliding failure.

### 5. Variation of 3D FS with Soil Parameters

To firmly establish the fact that the consideration of proper extent of 3<sup>rd</sup> dimension of the slope is of utmost importance during 3D slope stability analysis, it is pertinent that convergence

behavior of FS3D must be studied when soil parameters are also varying.

For this purpose, the effect of soil characteristics on the evaluated FS values of the 3D slope has been investigated to check the convergence of FS3D. Note that, in this study, five combinations of  $C'$ ,  $\phi'$  have been considered for three different geometric configurations of the slope, i.e., 1V:1.5H, 1V:1H and vertical cut. The slope angles for these cases are  $\beta = 33.69^\circ$ ,  $45.0^\circ$  and  $90^\circ$  respectively. The different combinations of  $C'$ ,  $\phi'$  and  $\gamma'$  are shown in Table 3. All these slope problems are analyzed for different loading combinations involving pore pressure and earthquake loadings. The pore pressure loadings on the slope are simulated considering two values of pore pressure ratio i.e.,  $r_u = 0.0$  and  $0.50$ .

Similarly, the seismic loading on the slope is simulated by applying an equivalent horizontal static loading. The different values  $k_{eq}$  considered in the present analyses are 0.0 and 0.20, respectively. Overall, two loading combinations have been considered for soil characteristics in the current work, out of which the case  $r_u = 0.0$  and  $k_{eq} = 0.0$  represents a soil slope subjected to only gravity loading. This investigation aims to check the convergence of 3D factor of safety at different soil characteristics. For this analysis, the convergence of 3D FS is checked at extreme loading conditions for different soil characteristics of soil slopes represented by  $r_u = 0.50$  and  $k_{eq} = 0.20$ .

Figure 13 presents the 3D factor of safety of different soil characteristics for a soil slope subjected to only gravity loading with varying inclinations of slopes (1V:1.5H and 1V:1H) as well as for different  $l/h$  ratios (where  $l$  is the length in the longitudinal direction and  $h$  is the height of the slope).

**Table 2.** Analysis of 2D and 3D safety factor for different parametric studies

Slope angle ( $\beta$ )	$r_u; k_{eq}$	FS (2D)	L/H	FS (3D)	Volume of failure soil (m <sup>3</sup> )
1V:3H (18.43°)	0.0; 0.0	2.008	5	2.188	5.828×10 <sup>4</sup>
	0.0; 0.0	2.008		2.188	5.828×10 <sup>4</sup>
	0.0; 0.05	1.727		1.868	6.066×10 <sup>4</sup>
	0.0; 0.10	1.513		1.626	6.127×10 <sup>4</sup>
	0.0; 0.15	1.335		1.437	6.272×10 <sup>4</sup>
	0.0; 0.20	1.199		1.287	6.362×10 <sup>4</sup>
	0.25; 0.0	1.716		1.875	6.462×10 <sup>4</sup>
	0.25; 0.05	1.478		1.598	6.562×10 <sup>4</sup>
	0.25; 0.10	1.294		1.390	6.751×10 <sup>4</sup>
	0.25; 0.15	1.141		1.228	6.758×10 <sup>4</sup>
	0.25; 0.20	1.024		1.099	6.839×10 <sup>4</sup>
	0.50; 0.0	1.429		1.548	7.549×10 <sup>4</sup>
	0.50; 0.05	1.224		1.319	7.379×10 <sup>4</sup>
	0.50; 0.10	1.069		1.146	7.379×10 <sup>4</sup>
	0.50; 0.15	0.948		1.012	7.467×10 <sup>4</sup>
	0.50; 0.20	0.850		.9057	7.467×10 <sup>4</sup>
1V:1.5H (33.69°)	0.0; 0.0	1.464	5	1.596	1.440×10 <sup>4</sup>
	0.0; 0.05	1.338		1.452	1.664×10 <sup>4</sup>
	0.0; 0.10	1.221		1.327	1.827×10 <sup>4</sup>
	0.0; 0.15	1.121		1.217	2.120×10 <sup>4</sup>
	0.0; 0.20	1.034		1.120	2.347×10 <sup>4</sup>
	0.25; 0.0	1.264		1.387	1.571×10 <sup>4</sup>
	0.25; 0.05	1.148		1.258	1.884×10 <sup>4</sup>
	0.25; 0.10	1.047		1.147	1.884×10 <sup>4</sup>
	0.25; 0.15	0.962		1.049	2.397×10 <sup>4</sup>
	0.25; 0.20	0.889		0.964	2.491×10 <sup>4</sup>
	0.50; 0.0	1.044		1.168	2.107×10 <sup>4</sup>
	0.50; 0.05	0.945		1.056	2.273×10 <sup>4</sup>
	0.50; 0.10	0.862		0.959	2.696×10 <sup>4</sup>
	0.50; 0.15	0.791		0.875	2.743×10 <sup>4</sup>
	0.50; 0.20	0.731		0.804	2.814×10 <sup>4</sup>
	1V:1H (45°)	0.0; 0.0		1.201	5
0.0; 0.05		1.121	1.269	7.473×10 <sup>3</sup>	
0.0; 0.10		1.049	1.182	8.421×10 <sup>3</sup>	
0.0; 0.15		0.986	1.103	8.581×10 <sup>3</sup>	
0.0; 0.20		0.928	1.030	1.041×10 <sup>4</sup>	
0.25; 0.0		1.034	1.185	7.314×10 <sup>3</sup>	
0.25; 0.05		0.964	1.101	8.253×10 <sup>3</sup>	
0.25; 0.10		0.902	1.024	9.102×10 <sup>3</sup>	
0.25; 0.15		0.846	0.955	9.523×10 <sup>3</sup>	
0.25; 0.20		0.796	0.890	1.099×10 <sup>4</sup>	
0.50; 0.0		0.862	1.025	7.948×10 <sup>3</sup>	
0.50; 0.05		0.804	0.926	8.517×10 <sup>3</sup>	
0.50; 0.10		0.752	0.861	1.011×10 <sup>4</sup>	
0.50; 0.15		0.706	0.801	1.154×10 <sup>4</sup>	
0.50; 0.20		0.665	0.746	1.278×10 <sup>4</sup>	
1V:0.5H (63.43°)		0.0; 0.0	0.922	5	
	0.0; 0.05	0.872	0.976		3.712×10 <sup>3</sup>
	0.0; 0.10	0.827	0.968		3.813×10 <sup>3</sup>
	0.0; 0.15	0.785	0.920		3.953×10 <sup>3</sup>
	0.0; 0.20	0.746	0.892		4.053×10 <sup>3</sup>
	0.25; 0.0	0.774	0.901		4.112×10 <sup>3</sup>
	0.25; 0.05	0.731	0.856		4.153×10 <sup>3</sup>
	0.25; 0.10	0.691	0.812		4.234×10 <sup>3</sup>
	0.25; 0.15	0.655	0.782		4.383×10 <sup>3</sup>
	0.25; 0.20	0.621	0.746		4.453×10 <sup>3</sup>
	0.50; 0.0	0.626	0.726		4.612×10 <sup>3</sup>
	0.50; 0.05	0.591	0.690		4.692×10 <sup>3</sup>
	0.50; 0.10	0.556	0.658		4.709×10 <sup>3</sup>
	0.50; 0.15	0.525	0.627		4.721×10 <sup>3</sup>
	0.50; 0.20	0.496	0.602		4.753×10 <sup>3</sup>

**Table 3.** Details of  $C'$ ,  $\phi'$  and  $\gamma'$  values

Parameter	Cases				
	C 1	C 2	C 3	C 4	C 5
$c'$ (kN/m <sup>2</sup> )	40	50	60	70	80
$\phi'$ (°)	20°	15°	10°	5°	0°
$\gamma'$ (kN/m <sup>3</sup> )	18.816	18.816	18.816	18.816	18.816

It is noticed that the 3D safety factor converges at  $l/h = 3.0$  or more. Similarly, the variation of 3D FS is presented for  $r_u = 0.50$  and  $k_{eq} = 0.20$  in Figure 14. In this case, similar observations regarding the convergence of FS3D can be made i.e., FS3D values converge when the longitudinal dimension  $l$  is at least equal to  $5h$ . Therefore, in general, it can be stated the

longitudinal dimension  $l$  should at least be considered five times the height of the slope ( $h$ ) to obtain correct 3D FS values.

Figure 15 presents the 3D critical failure surface for Case 1 of vertical cut under gravity loading only ( $r_u = 0.0$ ;  $k_{eq} = 0.0$ ). The nature of the failure is observed to be compatible with toe failure.

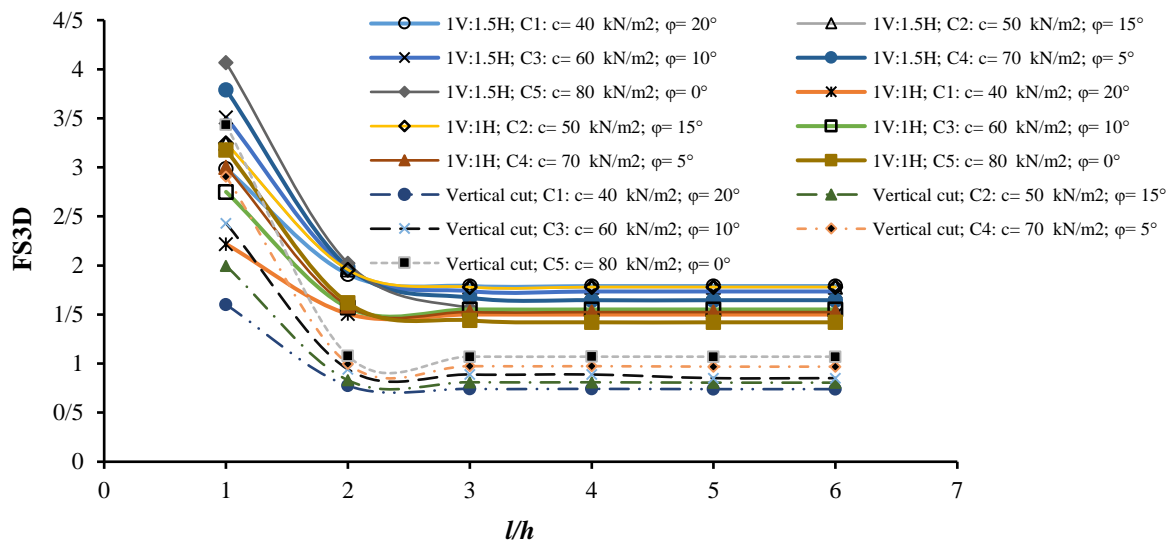


**Fig. 13.** Variation of FS3D with different  $l/h$  ratios having different soil properties ( $r_u = 0.0$ ,  $k_{eq} = 0.0$ )

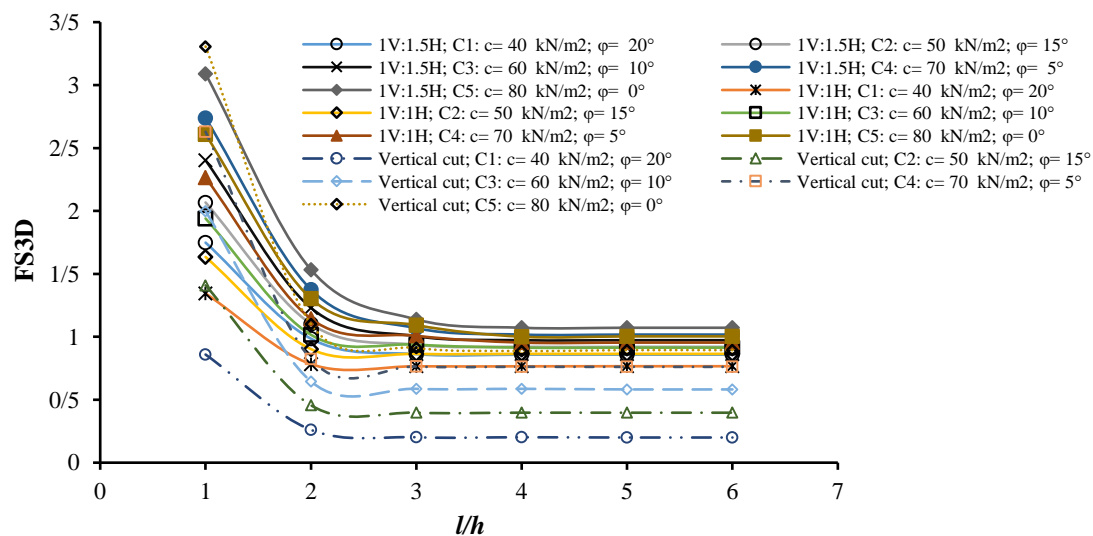


**Fig. 14.** Variation of FS3D with different  $l/h$  ratios having different soil properties ( $r_u = 0.50$ ,  $k_{eq} = 0.20$ )

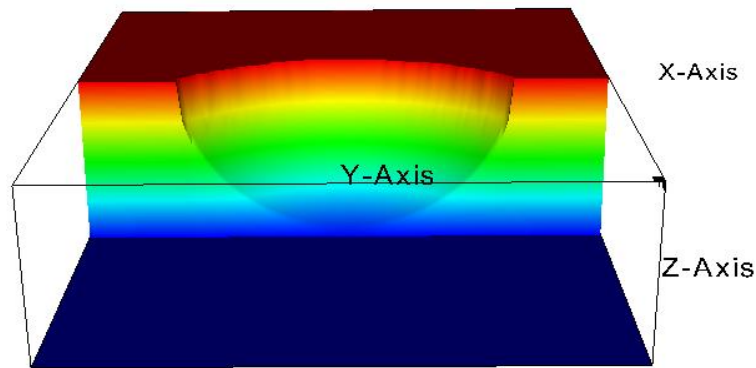


Fig. 15. 3D critical failure surface for Case 1 of vertical cut under gravity loading ( $r_u = 0.0$ ,  $k_{eq} = 0.0$ )

## 6. Conclusions

During 3D slope stability analysis, fixing the longitudinal direction of the 3D slope model is a very important task. If the longitudinal dimension of the 3D slope model is selected incorrectly, the 3D slope stability analysis will produce the wrong results. The present paper recommended the longitudinal dimension of a 3D slope by observing the convergence behavior of the ratios FS3D and FS2D.

Based on Bishop's simplified analysis, the limit equilibrium technique was used to determine FS2D. On the other hand, FS3D was determined using a 3D extension of Bishop's simplified method through the Scoops-3D computer program of the USGS. The effects of pore pressure loading were incorporated by considering different pore pressure ratios ( $r_u = 0.0, 0.25$ , and  $0.50$ , respectively).

The effects of seismic loading were simulated in the analysis by considering different values of horizontal seismic coefficients, i.e.,  $k_h = k_{eq} = 0.0, 0.05, 0.10, 0.15, 0.20$ , etc.

Altogether, 15 loading combination cases were analyzed to study the variation of the ratio of  $\eta = \text{FS3D}/\text{FS2D}$  concerning  $l/h$  values for slopes with different inclination angles ( $\beta$ ). The above study yielded the following findings:

- It is observed that  $\eta$  converges satisfactorily for all loading combination cases at  $l/h = 5.0$ .
- The rate of convergence  $\eta$  is faster for steeper slopes and vice-versa.

- The third/longitudinal dimension of the 3D slope model should be considered equal to five times the height of the slope.
- The 2D and 3D safety factors decrease as the slope angle increases for a certain  $l/h$  ratio.
- Thus, decrease in the safety factor results from a reduction of the longitudinal extent of the sliding mass. Similarly, the volume of the failure mass from 3D slope analyses decreases simultaneously as the slope angle increases.
- As the resisting force develops along the entire failure mass, there is a corresponding decrease in the generated resisting moment, resulting in an overall decrease in the factor of safety against slope failure.
- For all analysis cases, the type of slope failure is also closely monitored. As the slope angle increases, the nature of the critical failure surface gradually transitions from base failure to toe failure.

## 7. Data Availability Statement

The authors state that all data related to the present work has been transparently provided in the manuscript. For any other queries, readers are requested to contact the corresponding author.

## 8. References

- Arai, K. and Tagyo, K. (1985). "Determination of noncircular slip surface giving the minimum factor of safety in slope stability analysis", *Soils and Foundations*, 25(1), 43-51, <https://doi.org/10.3208/sandf1972.25.43>.
- Arellano, D. and Stark, T.D. (2000). "Importance of

- three-dimensional slope stability analyses in practice", In *Proceedings of Sessions of Geo-Denver 2000-Slope Stability 2000*, (Vol. 289, pp. 18-32), [https://doi.org/10.1061/40512\(289\)2](https://doi.org/10.1061/40512(289)2).
- Baligh, M.M. and Azzouz, A.S. (1975). "End effects on stability of cohesive slopes", *ASCE Journal of the Geotechnical Engineering Division*, 101(11), 1105-1117, <https://doi.org/10.3313/jls1964.23.16>.
- Bishop, A.W. (1955). "The use of the slip circle in the stability analysis of slopes", *Geotechnique*, 5(1), 7-17, <https://doi.org/10.1680/geot.1955.5.1.7>.
- Cavounidis, S. (1988). "An extension of Bishop's simplified method of slope stability analysis to three dimensions", *Geotechnique*, 38(1), 155-156, <https://doi.org/10.1680/geot.1988.38.1.155>.
- Chakraborty, A. and Goswami, D. (2021). "Three-dimensional (3D) slope stability analysis using stability charts", *International Journal of Geotechnical Engineering*, 15(5), 642-649, <https://doi.org/10.1080/19386362.2018.145743>.
- Chugh, A.K. (2003). "On the boundary conditions in slope stability analysis", *International Journal for Numerical and Analytical Methods in Geomechanics*, 27(11), 905926, <https://doi.org/10.1002/nag.305>.
- Cornforth, D.H. (2005). *Landslides in practice*, Jhon Wiley & Sons, New Jersey.
- Dawson, E.M. and Roth, W.H. (1999). *Slope stability analysis with FLAC*, In *FLAC and Numerical Modeling in Geomechanics*, (pp. 3-9), CRC Press, <https://doi.org/10.1201/9781003078531-2>.
- Deng, D., Zhao, L. and Li, L. (2015). "Limit equilibrium slope stability analysis using the nonlinear strength failure criterion", *Canadian Geotechnical Journal*, 52(5), 563-576, <https://doi.org/10.1139/cgj-2014-0111>.
- Duncan, J.M. (1996). "State of the art: limit equilibrium and finite-element analysis of slopes", *Journal of Geotechnical Engineering*, 122(7), 577-596, [https://doi.org/10.1061/\(ASCE\)0733-9410\(1996\)122:7\(577\)](https://doi.org/10.1061/(ASCE)0733-9410(1996)122:7(577)).
- He, Y., Liu, Y., Zhang, Y. and Yuan, R. (2019). "Stability assessment of three-dimensional slopes with cracks", *Engineering Geology*, 252, 136-144, <https://doi.org/10.1016/j.enggeo.2019.03.001>.
- Huang, C.C., Tsai, C.C. and Chen, Y.H. (2002). "Generalized method for three-dimensional slope stability analysis", *Journal of Geotechnical and Geoenvironmental Engineering*, 128(10), 836-848, [https://doi.org/10.1061/\(asce\)10900241\(2002\)128:10\(836\)](https://doi.org/10.1061/(asce)10900241(2002)128:10(836)).
- Janbu, N. (1973). *Slope stability computations*, Wiley (John) & Sons, Incorporated, [https://doi.org/10.1016/0148-9062\(75\)90139-4](https://doi.org/10.1016/0148-9062(75)90139-4).
- Johari, A. and Mousavi, S. (2019). "An analytical probabilistic analysis of slopes based on limit equilibrium methods", *Bulletin of Engineering Geology and the Environment*, 78, 4333-4347, <https://doi.org/10.1007/s10064-018-1408-1>.
- Kalantari, B. and Pourkhosravani, A. (2011). "A review of current methods for slope stability evaluation", *Electronic Journal of Geotechnical Engineering*, 16, 1245-1254.
- Komasi, M. and Beiranvand, B. (2021). "Seepage and stability analysis of the Eyvashan Earth Dam under drawdown conditions", *Civil Engineering Infrastructures Journal*, 54(2), 205-223, <https://doi.org/10.22059/cej.2020.293429.1634>.
- Kumar, S., Choudhary, S.S. and Burman, A. (2023a). "Recent advances in 3D slope stability analysis: A detailed review", *Modeling Earth Systems and Environment*, 9(2), 14451462, <https://doi.org/10.1007/s40808-022-01597-y>.
- Kumar, S., Choudhary, S.S. and Burman, A. (2023b). "The effect of slope height and angle on the safety factor and modes of failure of 3D slopes analysis using limit equilibrium method", *Beni-Suef University Journal of Basic and Applied Sciences*, 12(1), 84, <https://doi.org/10.1186/s43088-023-00423-3>.
- Li, A.J., Merifield, R.S. and Lyamin, A.V. (2010). "Three-dimensional stability charts for slopes based on limit analysis methods", *Canadian Geotechnical Journal*, 47(12), 1316-1334, <https://doi.org/10.1139/T10-030>.
- Lin, H.D., Wang, W.C. and Li, A.J. (2020). "Investigation of dilatancy angle effects on slope stability using the 3D finite element method strength reduction technique", *Computers and Geotechnics*, 118, 103295, <https://doi.org/10.1016/j.compgeo.2019.103295>.
- Liu, X., Li, D.Q., Cao, Z.J. and Wang, Y. (2020). "Adaptive Monte Carlo simulation method for system reliability analysis of slope stability based on limit equilibrium methods", *Engineering Geology*, 264, 105384, <https://doi.org/10.1016/j.enggeo.2019.105384>.
- Lorig, L. (1999). *Lessons learned from slope stability studies*, In *FLAC and Numerical Modeling in Geomechanics*, (pp.1722), CRC Press, <https://doi.org/10.1201/9781003078531-4>.
- Loukidis, D., Bandini, P. and Salgado, R. (2003). "Comparative study of limit equilibrium, limit analysis and finite element analysis of the seismic stability of slopes", *Geotechnique*, 53(5), 463-479, <https://doi.org/10.1007/s12040-019-1314-3>.
- Lyamin, A.V. and Sloan, S.W. (2002). "Lower bound limit analysis using non-linear programming", *International Journal for Numerical Methods in Engineering*, 55(5), 573-611, <https://doi.org/10.1002/nme.511>.
- Michalowski, R.L. (2002). "Stability charts for



- uniform slopes", *Journal of Geotechnical and Geoenvironmental Engineering*, 128(4), 351-355, [https://doi.org/10.1061/\(ASCE\)1090-0241\(2002\)128:4\(351\)](https://doi.org/10.1061/(ASCE)1090-0241(2002)128:4(351)).
- Michalowski, R.L. (2010). "Limit analysis and stability charts for 3D slope failures", *Journal of Geotechnical and Geoenvironmental Engineering*, 136(4), 583593, [https://doi.org/10.1061/\(asce\)gt.1943-5606.0000251](https://doi.org/10.1061/(asce)gt.1943-5606.0000251).
- Qi, S., Ling, D., Yao, Q., Lu, G., Yang, X. and Zhou, J.W. (2021). "Evaluating slope stability with 3D limit equilibrium technique and its application to landfill in China", *Engineering Geology*, 280, 105939, <https://doi.org/10.1016/j.enggeo.2020.105939>.
- Qian, Z. G., Li, A.J., Chen, W.C., Lyamin, A.V. and Jiang, J.C. (2019). "An artificial neural network approach to inhomogeneous soil slope stability predictions based on limit analysis methods", *Soils and Foundations*, 59(2), 556-569, <https://doi.org/10.1016/j.sandf.2018.10.008>.
- Qin, C.B., Chian, S.C. and Gazetas, G. (2019). "Kinematic analysis of seismic slope stability with discretisation technique and pseudo-dynamic approach: A new perspective", *Geotechnique*, 69(11), 1031-1033, <https://doi.org/10.1680/jgeot.18.D.011>.
- Rao, B., Burman, A. and Roy, L.B. (2023). "An efficient box search method for limit equilibrium method-based 3D slope stability analysis", *Transportation Infrastructure Geotechnology*, 11(1), 327-358, <https://doi.org/10.1007/s40515-023-00285-3>.
- Reid, M.E., Christian, S.B., Brien, D.L. and Henderson, S. (2015). *Scoops3D-software to analyze three-dimensional slope stability throughout a digital landscape*, (No. 14-A1), U.S. Geological Survey.
- Soralump, S., Panthi, K. and Prempramote, S. (2021). "Assessment of the upstream slope failure of a dam due to repeated cyclic drawdown", *Soils and Foundations*, 61(5), 13861398, <https://doi.org/10.1016/j.sandf.2021.08.006>.
- Su, Z. and Shao, L. (2021). "A three-dimensional slope stability analysis method based on finite element method stress analysis", *Engineering Geology*, 280, 105910, <https://doi.org/10.1016/j.enggeo.2020.105910>.
- Tozato, K., Dolojan, N.L. J., Touge, Y., Kure, S., Moriguchi, S., Kawagoe, S., Terada, K. (2022). "Limit equilibrium method-based 3D slope stability analysis for wide area considering influence of rainfall", *Engineering Geology*, 308, 106808, <https://doi.org/10.1016/j.enggeo.2022.106808>.
- Wang, L., Sun, D. and Li, L. (2019). "Three-dimensional, stability of compound slope using limit analysis method", *Canadian Geotechnical Journal*, 56(1), 116-125, <https://doi.org/10.1139/cgj-2017-0345>.
- Wang, L., Sun, D., Yao, Y., Wu, L. and Xu, Y. (2020). "Kinematic limit analysis of three-dimensional unsaturated soil slopes reinforced with a row of piles", *Computers and Geotechnics*, 120, 103428, <https://doi.org/10.1016/j.compgeo.2019.103428>.
- Xie, M., Esaki, T., Qiu, C. and Wang, C. (2006). Geographical information system-based computational implementation and application of spatial three-dimensional slope stability analysis", *Computers and Geotechnics*, 33(4-5), 260-274, <https://doi.org/10.1016/j.compgeo.2006.07.003>.
- Xu, Y., Zhao, M. wei, Lu, J., Wang, C., Jiang, L., Yang, C. and Huang, X.I. (2022). "Methods for the construction of DEM is of artificial slopes considering morphological features and semantic information", *Journal of Mountain Science*, 19(2), 563-577, <https://doi.org/10.1007/s11629-021-6831-2>.
- Yuan, W.H., Liu, K., Zhang, W., Dai, B. and Wang, Y. (2020). "Dynamic modeling of large deformation slope failure using smoothed particle finite element method", *Landslides*, 17(7), 1591-1603, <https://doi.org/10.1007/s10346-020-01375-w>.
- Zheng, Y., Chen, C., Liu, T., Zhang, H., Xia, K. and Liu, F. (2018). "Study on the mechanisms of flexural toppling failure in anti-inclined rock slopes using numerical and limit equilibrium models", *Engineering Geology*, 237, 116-128, <https://doi.org/10.1016/j.enggeo.2018.02.006>.



This article is an open-access article distributed under the terms and conditions of the Creative Commons Attribution (CC-BY) license.